Available online at www.sciencedirect.com
SCIENCE DIRECT®
PERGAMON
International Journal of Heat and Mass Transfer 46 (2003) 1553–1562
International Journal of HEAT and MASS TRANSFER
www.elsevier.com/locate/ijhmt

Three-dimensional numerical optimization of a manifold microchannel heat sink

J.H. Ryu, D.H. Choi *, S.J. Kim

Department of Mechanical Engineering, Korea Advanced Institute of Science and Technology, Taejon 305-701, Republic of Korea

Received 12 June 2002; received in revised form 7 October 2002

Abstract

A three-dimensional analysis procedure for the thermal performance of a manifold microchannel heat sink has been developed and applied to optimize the heat-sink design. The system of fully elliptic equations, that govern the flow and thermal fields, are solved by a SIMPLE-type finite volume method, while the optimal geometric shape is traced by a steepest descent technique. For a given pumping power, the optimal design variables that minimize the thermal resistance are obtained iteratively. The procedure is robust and the optimal state is reached within six global iterations. Comparing with the comparable traditional microchannel heat sink, the thermal resistance is reduced by more than a half while the temperature uniformity on the heated wall is improved by tenfold. The sensitivity of the thermal performance on each design variable is also examined and presented in the paper. Among various design variables, the channel width and depth are more crucial than others to the heat-sink performance. The optimal dimensions and corresponding thermal resistance have a power-law dependence on the pumping power.

1. Introduction

The recent trend in the electronic equipment industry toward denser and more powerful products requires higher thermal performance from a cooling technique. Many ideas for innovative cooling methods have been proposed including a microchannel heat sink. Two representative types of the microchannel heat sink are (1) the traditional microchannel (TMC) type and (2) the manifold microchannel (MMC) type. A TMC heat sink, which was proposed first by Tuckerman and Pease [1], is characterized by the long microchannels that run in one direction parallel to the heat-sink base. It has been successfully investigated by using a simple one-dimensional model [2] or more sophisticated three-dimensional numerical methods [3,4]. Even though the TMC heat sink has brought substantial improvements in the cooling performance, it has two disadvantages: the relatively high pressure loss and the significant temperature variation within the heat source. An MMC heat sink, on the other hand, differs from a TMC type in that the coolant flows through the alternating inlet and outlet manifolds in the direction normal to the heat-sink base to and from the segmented microchannels as shown in Fig. 1(a). The flow path is greatly reduced to a small fraction of the total length of a heat sink; the shortened flow path is expected to reduce the pressure drop and restrain the growth of the thermal boundary layer along the streamwise direction.

Harpole and Eninger [5] proposed an MMC system having between 10 and 30 manifold channels and reported that, for constant flow rate or pumping power, the maximum temperature and the temperature variation within the heat source were substantially reduced from that of a TMC heat sink. Copeland et al. [6] tested a variety of MMCs experimentally and reported that the thermal resistance was inversely proportional to the volume flow rate in a log–log scale. Copeland et al. [7] also found in a comparative study of an MMC heat sink

* Corresponding author. Tel.: +82-42-869-3018; fax: +82-42-869-3210.
E-mail address: dhchoi@mail.kaist.ac.kr (D.H. Choi).

0017-9310/03/$ - see front matter © 2002 Elsevier Science Ltd. All rights reserved.
PII: S0017-9310(02)00443-X

Nomenclature

c_p	heat capacity of fluid
D_h	hydraulic diameter of the channel, $2w_cH/(w_c+H)$
h	heat transfer coefficient defined in Eq. (9)
H	channel depth
k	thermal conductivity
$L \times W$	dimension of a heat sink
$M_{dv}, M_{in}, M_{out}, M_{tot}$	manifold dimensions (see Fig. 1)
N	number of channels
p	pressure
P	pumping power, $Q\Delta p$
Pr	Prandtl number, $\mu c_p/k_f$
$\dot{q}$	total heat-flow rate loaded on the bottom wall
q_w	heat flux loaded on the bottom wall
Q	total volume flow rate
Re	Reynolds number, $\rho U D_h/\mu$
R_t	thermal resistance
$\mathbf{S}$	search direction vector
T	temperature
ΔT_{max}	maximum temperature difference in a heat sink
$\vec{u}$	velocity vector in the fluid region
U	average velocity in the channel
w_c	channel width
W_w	fin thickness
w	$w_c + w_w$
x, y, z	cartesian coordinates
$\mathbf{X}$	design variable vector

Greek symbols

δ	substrate thickness
θ	nondimensionalized temperature
μ	fluid viscosity
ρ	fluid density
γ	inlet/outlet width ratio, M_{in}/M_{out}

Superscript

$*$	nondimensionalized variable

Subscripts

cf	channel floor
f	fluid
in	inlet
max	maximum
out	outlet
s	solid

that the simple analytical model based on correlations for a straight channel is not satisfactory in predicting the performance.

The purpose of the present study is to develop a three-dimensional analysis procedure for the thermal performance of an MMC heat sink and apply it to optimize the geometric shape and the operating condition. The SIMPLE-type finite volume method is coupled with an optimization scheme based on the steepest descent method [8]. The geometric parameters that minimize the thermal resistance are obtained. The effects of the channel number and the pumping power on the performance of a heat sink are examined.

2. Numerical analysis

The problem under consideration concerns the forced convection through the MMC heat sink depicted in Fig. 1(a). A coolant, guided by the inlet, divider, and outlet manifolds, passes through a number of microchannels and takes heat away from an electronic component attached below. In analyzing the problem, it is assumed that the flow is laminar, incompressible, and all thermophysical properties are constant.

Due to the periodicity, it suffices to consider only a single periodic module of the geometry, that includes the flow passage, the substrate, the fin, and the manifold divider, shown in Fig. 1(b). The nondimensionalized continuity, Navier–Stokes, and energy equations in three dimensions that govern the flow may be written as

Continuity equation:

$$\nabla^* \cdot \vec{u}^* = 0 \tag{1}$$

Momentum equation:

$$\vec{u}^* \cdot \nabla^* \vec{u}^* = -\nabla^* p^* + \frac{1}{Re}\nabla^{*^2}\vec{u}^* \tag{2}$$

Energy equation:

$$\vec{u}^* \cdot \nabla^* \theta = \frac{1}{Re\,Pr}\nabla^{*^2}\theta \quad \text{(fluid region)} \tag{3}$$

$$0 = \nabla^{*^2}\theta \quad \text{(solid region)} \tag{4}$$

where

$$Re = \frac{\rho U D_h}{\mu}, \quad Pr = \frac{\mu c_p}{k_f},$$
$$\nabla^* = D_h\nabla, \quad \vec{u}^* = \vec{u}/U, \quad p^* = p/\rho U^2,$$
$$\theta = \frac{T - T_{f,in}}{q_w D_h/k_s} \tag{5}$$

Here $\vec{u}$, U, p, and T are the velocity vector, the mean velocity in the channel, the pressure, and the temperature, respectively. The fluid properties, ρ, μ, k, and c_p

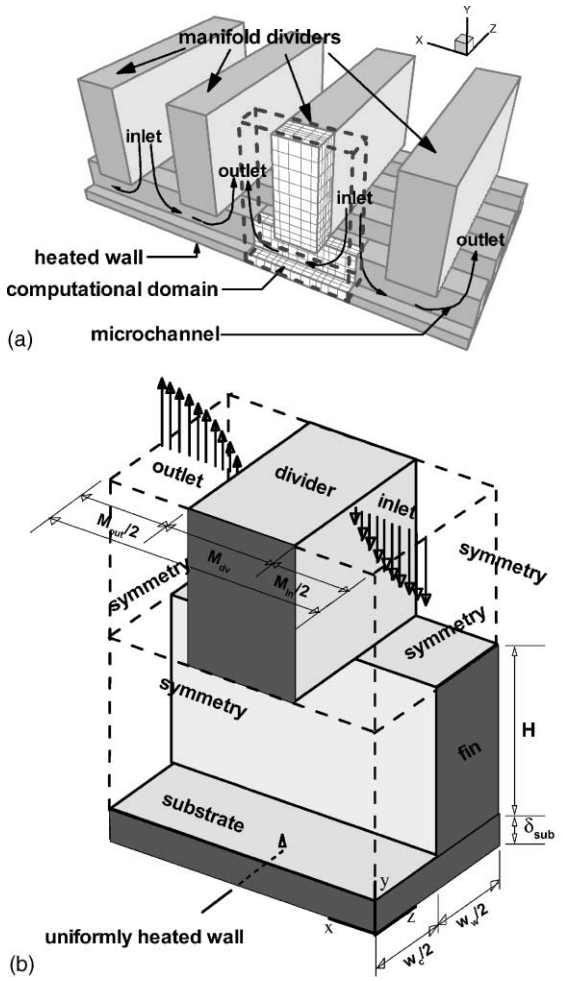

Fig. 1. Schematic of an MMC heat sink: (a) general configuration and (b) computational domain and boundary conditions.

represent the density, viscosity, conductivity, and the heat capacity. The characteristic length D_h is the hydraulic diameter of the channel and q_w the heat flux loaded on the bottom wall, while the subscript f and s denote the fluid and solid phases, respectively.

Fig. 1(b) describes the boundary conditions of the present computational domain. The symmetry condition is imposed for both velocity and temperature at four planes of symmetry, i.e., $x = 0, x_{max}$ and $z = 0, z_{max}$. The velocities at the inlet and the outlet are assumed to be fully developed, as the boundaries are sufficiently far from the microchannels. The coolant enters the MMC heat sink with a prescribed temperature ($T_{f,in}$) and exits adiabatically. A uniform heat flux, q_w, is applied to the bottom wall of the substrate attached to the heat-generating component. The upper boundary of the divider is also treated as adiabatic.

The Eqs. (1)–(4) are then solved by a finite volume method of SIMPLE-type in which an upwind differencing scheme is used for the convective derivatives. The process is iterative and the solution is considered converged when the sums of the mass sources and the temperature variations between the two successive iterations for the entire region become less than 10^{-3} and 10^{-2}, respectively. A nonuniformly distributed $22 \times 21 \times 16$ grid is found to be adequate and has been used throughout the study, since the result is in good agreement with that obtained with a $44 \times 42 \times 32$ grid, as will be seen later in Fig. 6.

3. Optimization technique

To maximize the thermal performance of an MMC heat sink, the geometric shape of a heat sink is optimized by using the steepest descent method [8]. The objective function to be minimized is the thermal resistance, a commonly used quantity in measuring the heat-sink performance,

$$R_t = \frac{\Delta T_{max}}{\dot{q}} = \frac{(T_{w,max} - T_{f,in})}{\dot{q}} \tag{6}$$

where $T_{w,max}$ and $T_{f,in}$ are the maximum wall temperature and the inlet fluid temperature, respectively, and $\dot{q}$ is the total heat-flow rate. The key geometric parameters of an MMC heat sink, namely, the channel depth H, the channel width w_c, the fin thickness w_w, and the inlet/outlet width ratio γ, are chosen as the design variables. The divider thickness, as well as the number of manifolds, too is an important parameter. Usually the narrower the divider, the better the thermal performance as the flow path becomes shorter. However, fabricating an extremely thin divider may be prohibitively expensive. Therefore, the divider thickness and the sum of inlet/outlet widths are restricted to be no smaller than 0.5 and 1 mm, respectively, for most of the present calculations. The optimization is carried out under the constraint of a given pumping power.

Starting with a specified set of design variables, $\mathbf{X}^0$, a new set of values is obtained at each iterative step:

$$\mathbf{X}^{n+1} = \mathbf{X}^n + l\mathbf{S}^n \tag{7}$$

where n is the iteration number and $\mathbf{S}$ is the directional vector in the design variable space. The scalar length l defines the distance that we wish to move in the direction of $\mathbf{S}$. In the steepest decent method, the direction $\mathbf{S}$ at the nth iteration is taken as the negative of the normalized gradient of the objective function:

$$\mathbf{S}^n = -\Delta R_t(\mathbf{X}^n)/|\Delta R_t(\mathbf{X}^n)| \tag{8}$$

Here the differentiation is done numerically by using two successive solutions in each direction. The maximum

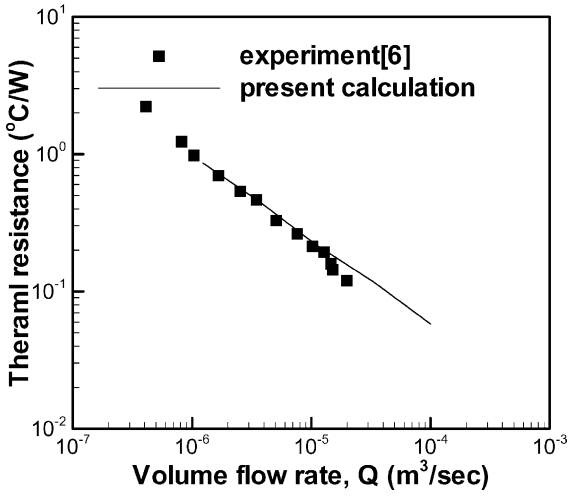

Fig. 2. Thermal resistance vs various flow rates for an MMC heat sink with $H = 150$ μm, $M_{in} = M_{out} = M_{dv} = 500$ μm, and $w_c = w_w = 57$ μm.

distance that l can take, called the move limit, is specified and used as an initial guess to obtain $\mathbf{X}^{n+1}$. The new solution field of Eqs. (1)–(4) for $\mathbf{X}^{n+1}$ is then computed. If R_t^{n+1} is smaller than R_t^n, we accept this $\mathbf{X}^{n+1}$ as the value at the $(n+1)$th iteration. Otherwise, a new $\mathbf{X}^{n+1}$ is tried using a shorter l until R_t^{n+1} meets the above criterion. No more than three local iterations were required to find $\mathbf{X}^{n+1}$. This completes one global iteration, and is repeated until the design variable vector $\mathbf{X}^n$ stays within the specified limit between the two successive iterations.

4. Results and discussion

We consider the heat sink which has a square horizontal surface $(L \times W)$, 1 cm × 1 cm. The water ($\rho = 1000$ kg/m^3, $\mu = 0.001$ kg/ms, $k_f = 0.613$ W/mK, $c_p = 4179$ J/kgK) and the silicon ($k_s = 148$ W/mK) are used as the coolant and the heat-sink material, respectively. The divider is usually made of copper ($k_s = 400$

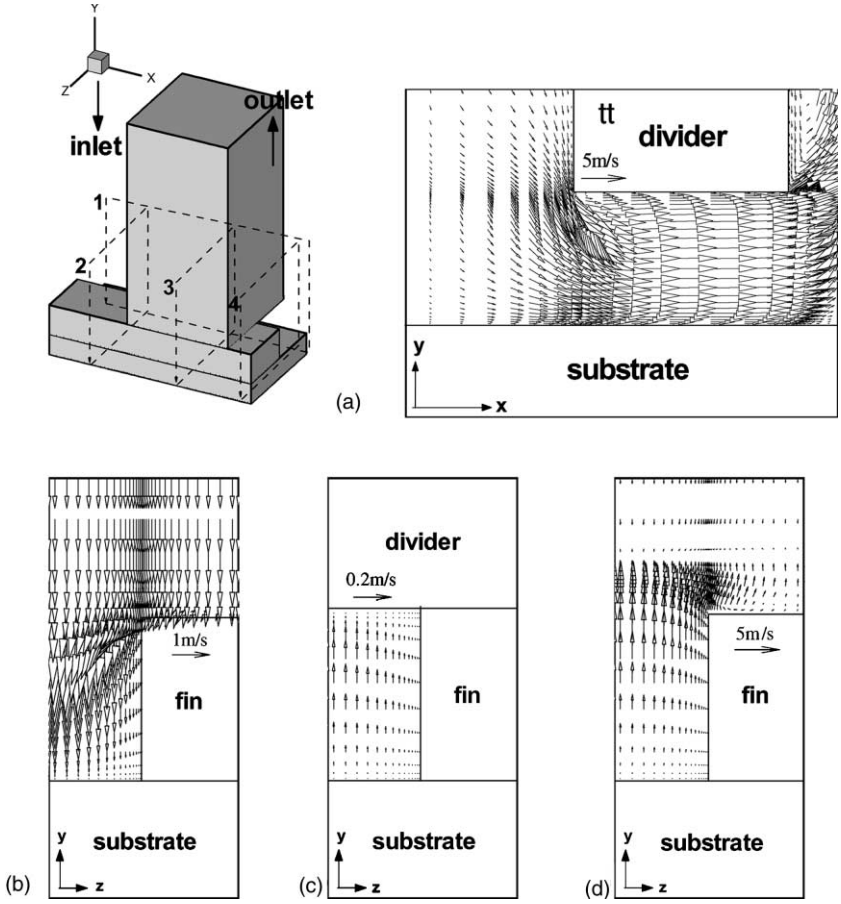

Fig. 3. Velocity vectors at the various planes in the MMC heat sink for $P = 2.56$ W, $H = 150$ m, $w_c = 16.0$ μm, $w_w = 16.4$ μm, $\delta = 100$ μm, $M_{in} = 772$ μm, $M_{dv} = 500$ μm, $M_{out} = 228$ μm: (a) channel centerplane, (b) $x/M_{tot} = 0.35$, (c) $x/M_{tot} = 0.65$, and (d) $x/M_{tot} = 0.90$.

W/mK) and is bonded to the microchannel heat sink. It is thus safe to assume that the contact resistance is negligible. To validate the numerical procedure, the thermal resistance over a wide range of flow rates is compared with earlier measurement [6], in which the coolant was fluorocarbon liquid FX-3250. Fig. 2 shows that the thermal resistance is inversely proportional to the volume flow rate in a log–log scale and is in good agreement with the experimental data. This confirms that the procedure developed in the present study is adequate for the numerical analysis.

The calculation is first performed for a given geometric shape and a pumping power to characterize the flow and heat transfer phenomena. The widths of inlet and outlet are 772 and 228 μm, respectively, while the divider thickness is 500 μm. The microchannel width, depth, and fin thickness are 16 μm, 150 μm, and 16.4 μm. This amounts to 309 fins on the component. The substrate thickness is 100 μm and the uniform heat flux of 10^2 W/cm^2 is applied at the bottom surface. The pumping power is 2.56 W, which results in the volume flow rate of 23.1 cm^3/s and $Re = 91$.

Fig. 3 shows the velocity vectors on the channel centerplane (a) and at various cross-sections (b)–(d) in the streamwise direction. Upon impinging on the channel floor, the flow accelerates rapidly and undergoes a drastic change as it enters the channel region due to a large reduction in the cross-sectional area. Since the flow path is short, the boundary layer is mostly in the developing stage, as can be manifested by the secondary flow in Fig. 3(b)–(d). Also shown in the figure is the acceleration of the flow around the corners and its ramification is discussed later.

The temperature field depicted in Fig. 4 exhibits how the cooling of the device proceeds: it is apparent that the cooling is most effective in the channel entrance region just past the stagnant zone directly under the inlet manifold. The thermal boundary layer grows as the coolant travels through the channel. The heat removal is most active where the thermal boundary layer is thinnest and, consequently, the temperature in the substrate is lowest there. This is clearly quantified in Figs. 5 and 6, where the heat flux across various cross-sections and the mean surface temperature along the channel are

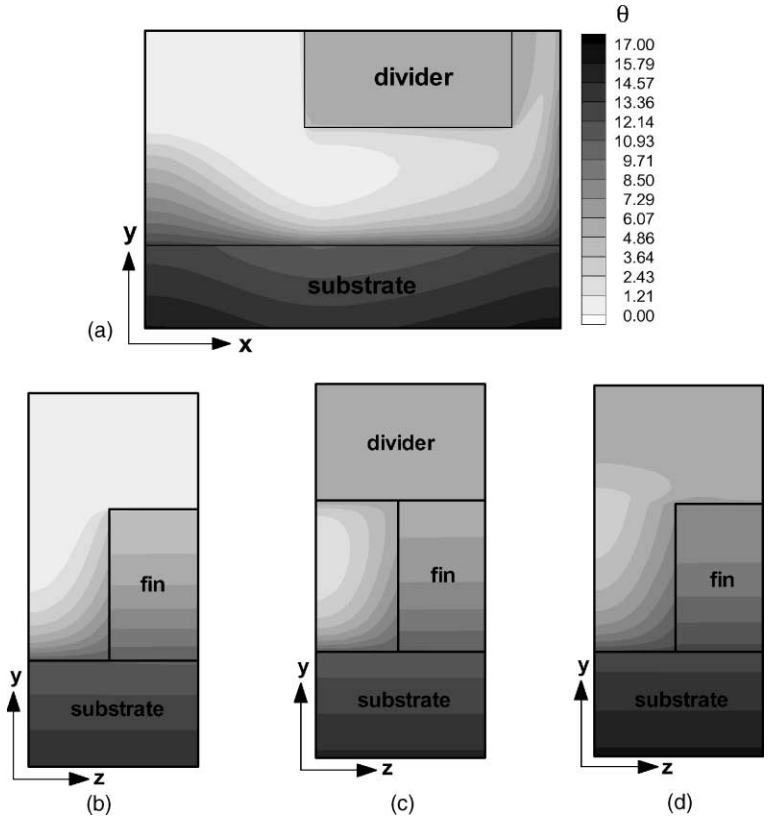

Fig. 4. Temperature contours at the various planes in the MMC heat sink for $P = 2.56$ W, $H = 150$ μm, $w_c = 16.0$ μm, $w_w = 16.4$ μm, $\delta = 100$ μm, $M_{in} = 772$ μm, $M_{dv} = 500$ μm, $M_{out} = 228$ μm: (a) channel centerplane, (b) $x/M_{tot} = 0.35$, (c) $x/M_{tot} = 0.65$, and (d) $x/M_{tot} = 0.90$.

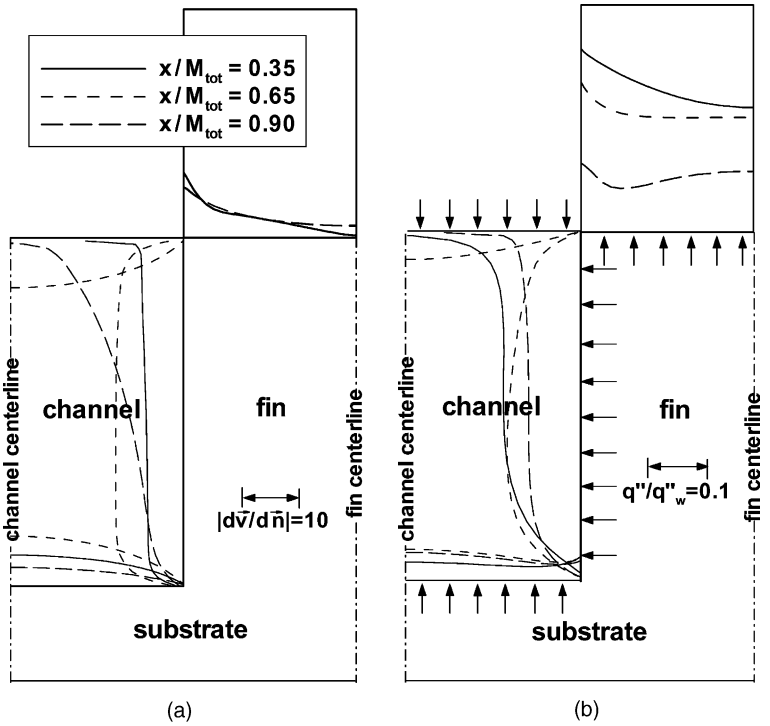

Fig. 5. Velocity gradient and heat flux at the channel wall and fin tip in the MMC heat sink for $P = 2.56$ W, $H = 150$ μm, $w_c = 16.0$ μm, $w_w = 16.4$ μm, $\delta = 100$ μm, $M_{in} = 772$ μm, $M_{dv} = 500$ μm, $M_{out} = 228$ μm: (a) velocity gradient and (b) heat flux.

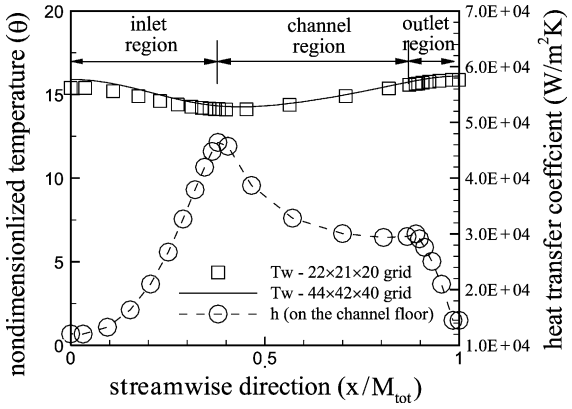

Fig. 6. Wall temperature and local heat transfer coefficient on the channel floor under the channel centerline along the streamwise direction.

presented. The magnitude of the velocity gradient and the heat flux on the surface are shown for three different cross-sections, i.e., $x/M_{tot} = 0.35$, 0.65, and 0.90. The middle one ($x/M_{tot} = 0.65$) is in the horizontal channel portion while the other two are in the inlet and outlet regions, respectively. Among the three cross-sections, both the velocity gradient and the heat flux are largest at $x/M_{tot} = 0.65$, as expected from Figs. 3 and 4. The rapid increase in the heat flux near the fin tip in the inlet/outlet regions is attributed to the acceleration of the fluid when going around the corner of the fin tip. The temperature distribution on the substrate is fairly uniform (Figs. 4 and 6) and the maximum temperature difference on the heated wall is much smaller than that of the comparable TMC heat sink (0.38 vs 4.27 °C) studied earlier [4]. It is also very informative to observe that the most of the heat (95%) is removed through the fin surface. Although the temperature of the channel floor is higher than that of the fin, the slowly moving fluid inside the thick boundary layer formed in the vicinity of the channel floor is not very effective in removing the heat from the substrate directly. Also shown in Fig. 6 is the heat transfer coefficient on the channel floor along the channel centerline. For the present configuration, the heat transfer coefficient is defined as

$$h = \frac{-k_f \frac{\partial T}{\partial y}\Big|_{cf}}{T_{cf} - T_{f,in}} \tag{9}$$

where the subscript cf denotes the channel floor. It increases rapidly in the streamwise direction until it has a maximum value near $x = 0.4M_{tot}$, which coincides with the location where the wall temperature attains its minimum value. Again, the thinning of the thermal boundary layer due to the flow acceleration resulting

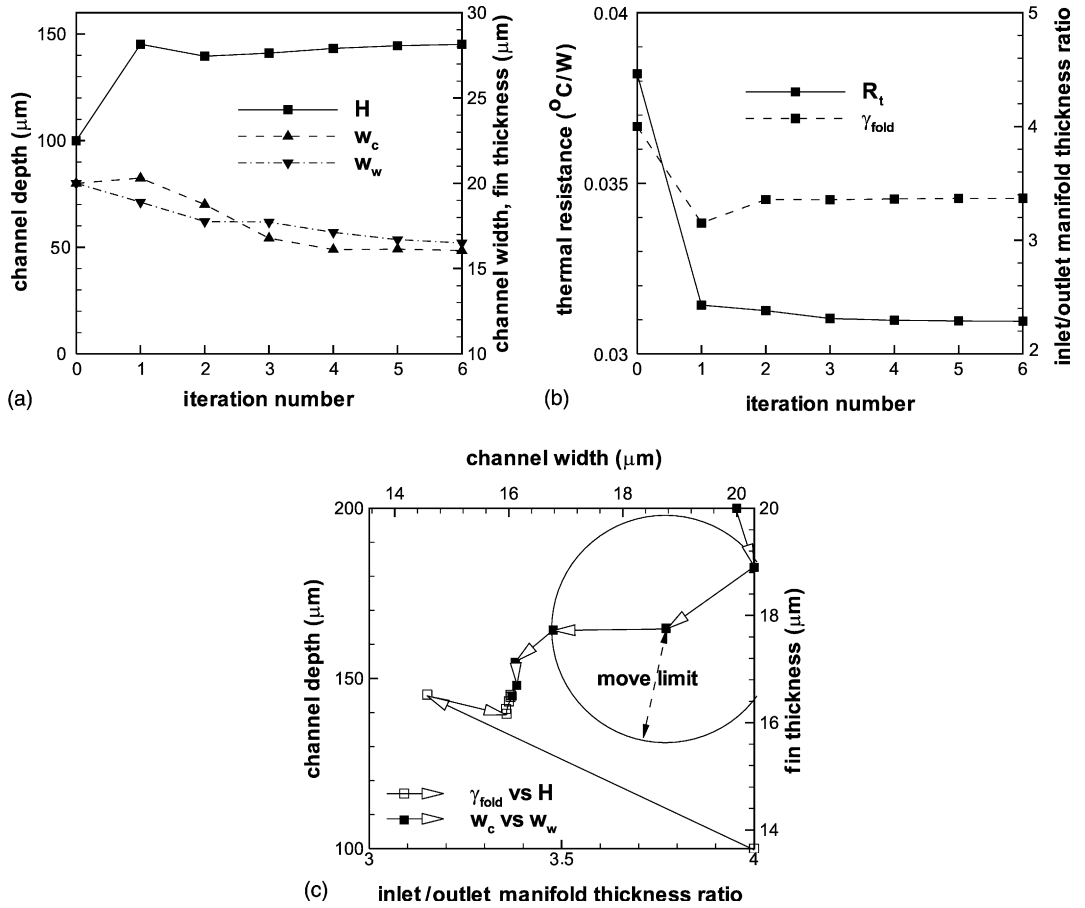

Fig. 7. Convergence history toward the optimal values: (a) channel dimensions, (b) inlet/outlet manifold thickness ratio and thermal resistance, and (c) moving trace toward the optimal point on the design variable space.

Table 1
Optimal results for various constraints on manifold thickness

Constraints	$M_{dv} \geqslant 500$ μm $M_{in} + M_{out} \geqslant 1000$ μm	$M_{dv} \geqslant 200$ μm $M_{in} + M_{out} \geqslant 400$ μm	$M_{dv} \geqslant 100$ μm $M_{in} + M_{out} \geqslant 200$ μm
R_t (°C/W)	3.10×10^{-2}	2.32×10^{-2}	1.96×10^{-2}

from the cross-sectional area reduction in the inlet region is responsible for this phenomenon. After reaching the maximum point, the heat transfer coefficient decreases monotonically because of the steady growth of the thermal boundary layer.

The optimization procedure described in the previous section is then used to obtain the optimal shape of an MMC heat sink. With an arbitrarily chosen initial guess, the optimal values of the design variables, i.e., the channel depth and width, the fin thickness, and the inlet/outlet width ratio, are estimated. The solution converges within six global iterations, despite the fact that the initial geometry is far from the final one, and the total computation time is less than 2 h on a PC with a Pentium IV (1.8 GHz) microprocessor. In the early stage of computation, the total number of channels is allowed to take a floating-point number. Once the calculation reaches the point when this number becomes stable and varies little, the number of channels is rounded to the nearest integer and fixed for further iteration. The convergence history for the design variables is given in Fig. 7. It is seen from the figure that there is definitely one optimal state, which happens to be the case presented above, for the given pumping power and that the search

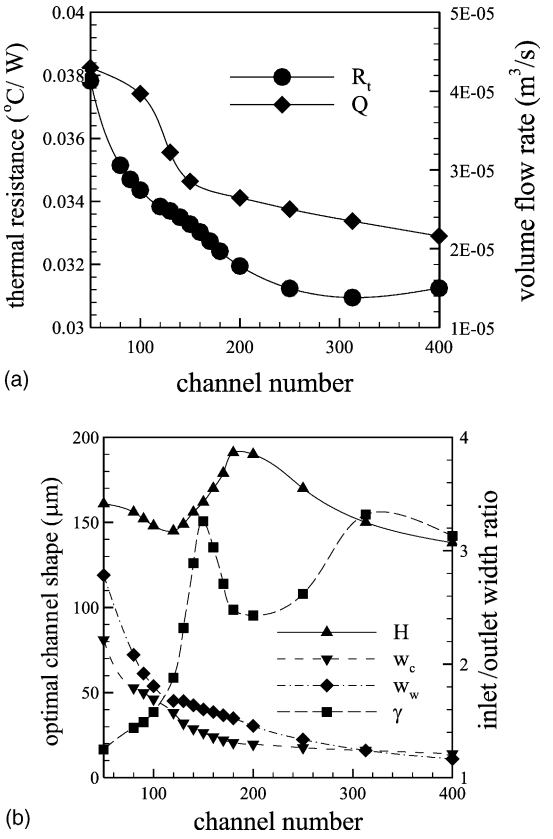

Fig. 8. Effect of the channel number on the thermal performance of an MMC heat sink: (a) optimal thermal resistance and volume flow rate and (b) optimal heat-sink shape.

technique works effectively to find that point in the design variable space. The convergence is nearly monotonic in that the first iteration seems most significant.

The thermal resistance for the optimal state is 3.10×10^{-2} °C/W which is less than a half of that of a comparable TMC heat sink quoted above [4]. It is appropriate to mention here that the thermal resistance of the MMC heat sink in the present study can be reduced further if we allow the divider thickness to go smaller, i.e., make the flow path shorter. Additional calculations have been carried out for two smaller divider thicknesses and the results, compared in Table 1, show clearly the downward trend of the thermal resistance with the narrowing divider.

To examine the sensitivity of the performance to the change in the design variable, we ran the optimization procedure with the channel number (N) fixed. Fig. 8 presents the optimal geometric shape and corresponding thermal resistance for various N. The thermal resistance increases monotonically, gradually first and then more steeply thereafter, as N decreases. While both the channel width and the fin thickness increase with decreasing N, the inlet/outlet width ratio and the channel depth exhibit some peculiar behavior. There appears to be two distinctly different flow regimes: one for $N < 120$ and the other for $N > 200$. The region in between is the transitional regime. For $N < 120$, the channel aspect ratio (H/w_c) is rather low (2–5), and the inlet to outlet width ratio is also moderate (<2). For $N > 200$, on the other hand, the channel aspect ratio becomes very high

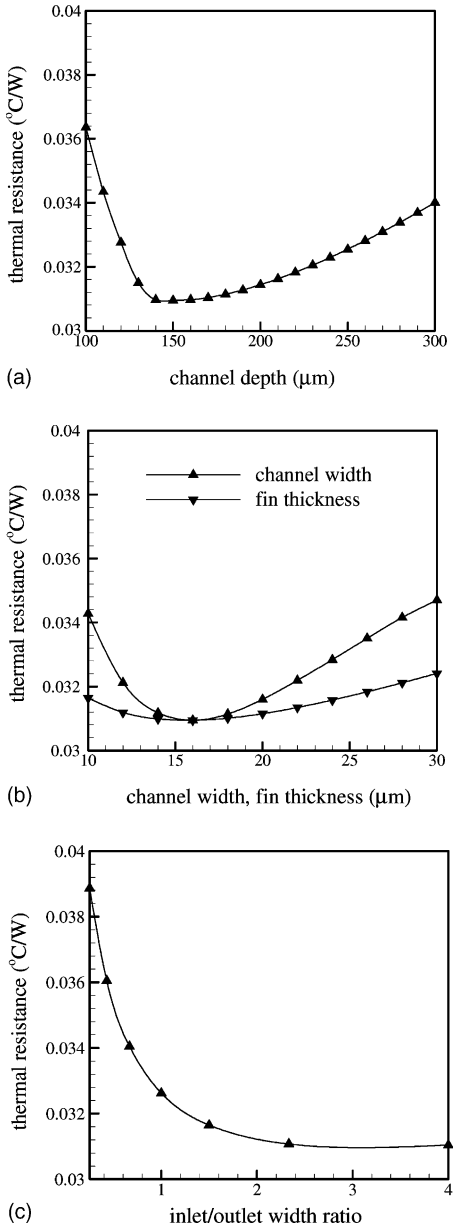

Fig. 9. Effects of each design parameter on the thermal resistance: (a) channel depth, (b) channel width and fin thickness, and (c) inlet/outlet width ratio.

(≈10) and so does the inlet to outlet width ratio (>2.5). The flow rate in the former regime is much larger than that of the latter due to lower friction and the improvement in the thermal resistance is also very steep with increasing N. However, as N increases further, the thermal resistance of the latter state becomes lower. The increase of the channel surface area and, hence the friction loss, reduces the flow rate abruptly; the variation in the thermal resistance is more gradual.

While the optimal geometric shape itself is important in the heat-sink performance, it is imperative to know the behavior in an off-design condition. The thermal resistance when each one of the design variables such as the channel depth (H), the channel width (w_c), and the fin thickness (w_w), is varied is presented in Fig. 9. The figure exhibits that the thermal resistance increases slowly when $H > H_{opt}$ but very rapidly when $H < H_{opt}$. The similar behavior may be observed in the variation of the channel width or the fin thickness. It should be noted that the channel number is varied according to the increasing/decreasing channel width and the fin thickness. One useful and interesting phenomenon displayed in the figure is that the performance deteriorates more rapidly when the channel width moves away from its optimum than when the fin thickness does. This indicates that keeping the channel width close to its optimal value is more crucial to the performance than maintaining the fin thickness when the channel number is altered. This is in line with the observation made in Fig. 8 and also in the earlier study about the TMC heat sink [4].

Finally, a series of calculation is carried out for various values of the pumping power. The varying pumping power assigns different Reynolds numbers in Eq. (3), which comes out as part of the solution. Similar effects can be attained when the size of the heat sink is made different. The results, plotted on a log–log scale in Fig. 10, show that both the optimal dimensions and the thermal resistance have a power-law dependence on the pumping power. The Reynolds number is the only relevant dimensionless parameter other than the Prandtl number and its relation with the pumping power is also linear in a log–log scale as shown in the figure.

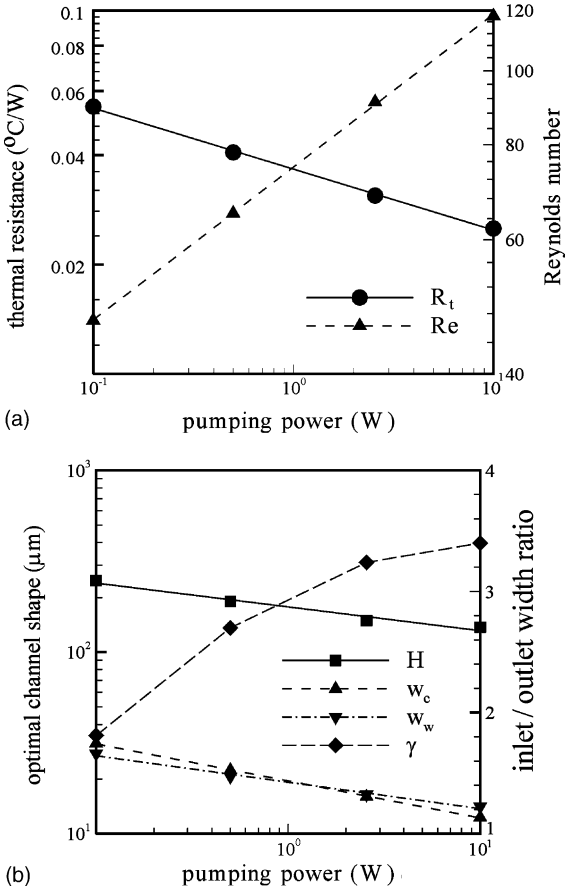

Fig. 10. Effect of the pumping power on the optimal thermal performance of an MMC heat sink: (a) optimal thermal resistance and Reynolds number and (b) optimal heat-sink shape.

5. Conclusions

A three-dimensional analysis procedure for the thermal performance of an MMC heat sink has been developed and coupled with the steepest descent algorithm to obtain the optimal geometric dimensions. For a given pumping power and a specified number of manifolds, the optimal channel depth, channel width, fin thickness, and inlet/outlet width ratio that yield the lowest thermal resistance are numerically calculated. The convergence is robust and the optimal state has been reached within six global iterations. It was found that 95% of the heat is removed through the fin surface and that the lowest temperature on the floor is attained in the vicinity of the channel entrance point while the hottest spots are near the inlet and outlet stagnation points in the channel floor. Comparing to the TMC heat sink for the identical heat load and pumping power, the thermal resistance is lowered by more than 50% while the maximum temperature variation on the heated wall is improved by tenfold.

Among various design variables, the channel width and depth appear to be more critical than others in dictating the heat-sink performance. When the channel number is allowed to vary, the optimal channel shape and flow rate change widely: the aspect ratio of the channel cross-section and the inlet to outlet width ratio are both low, and carries a larger flow rate when the channel density is relatively sparse while the opposite is true when the channel number exceeds 200. The optimal

dimensions and corresponding thermal resistance have a power-law dependence on the pumping power. The optimal aspect ratio of the channel cross-section remains unchanged as the Reynolds number of the pumping power varies.

Acknowledgements

This work was supported by KISTEP under Grant 2-578 through the National Research Lab. Program and, in part, by the Ministry of Education under the BK21 Project.

References

[1] D.B. Tuckerman, R.F.W. Pease, High-performance heat sinking for VLSI, IEEE Electr. Device Lett. 2 (1981) 126–129.

[2] S.J. Kim, D. Kim, Forced convection in microstructures for electronic equipment cooling, ASME J. Heat Transfer 121 (1999) 639–645.

[3] K. Vafai, L. Zhu, Analysis of two-layered microchannel heat sink concept in electronic cooling, Int. J. Heat Mass Transfer 42 (1999) 2287–2297.

[4] J.H. Ryu, D.H. Choi, S.J. Kim, Numerical optimization of the thermal performance of a microchannel heat sink, Int. J. Heat Mass Transfer 45 (2002) 2823–2827.

[5] G.M. Harpole, J.E. Eninger, Microchannel heat exchanger optimization, in: Proc. 7th IEEE Semi-Therm Symp., 1991, pp. 59–63.

[6] D. Copeland, H. Takahira, W. Nakayama, Manifold microchannel heat sinks: theory and experiments, Therm. Sci. Eng. 3 (2) (1995) 9–15.

[7] D. Copeland, M. Behnia, W. Nakayama, Manifold microchannel heat sinks: isothermal analysis, IEEE Trans. on Components, Packaging, and Manufacturing Technology—Part A 20 (2) (1997) 96–102.

[8] G.N. Vanderplaats, Numerical Optimization Techniques for Engineering Design, McGraw-Hill, New York, 1984 (Chapter 3).